 doi:10.20944/preprints201809.0605.v1

Article

Adsorption of carbon dioxide into amine functionalized ordered mesoporous materials

Marcela N. Barbosa [1,*], Maria J. F. Costa [1], Maricele N. Barbosa [1], Valter J. Fernandes Jr. [1], Giancarlo R. Salazar-Banda [2], Ana C. F. Coriolano [3], Álvaro Reyes-Carmona [4], Enrique Rodríguez-Castellón [4] and Antonio S. Araujo [1,*]

[1] Federal University of Rio Grande do Norte, Institute of Chemistry; 59078-970, Natal RN, Brazil; mnbarbosa@gmail.com (M.N.B.); mariacosta.ufrn@gmail.com (M.J.F.C.); maricelebarbosa@yahoo.com.br (M.N.B.); valter.ufrn@gmail.com (V.J.F.); araujo.ufrn@gmail.com (A.S.A).
[2] Tiradentes University, Research and Technology Institute, 49032-490, Aracaju SE Brazil; gianrsb@gmail.com (G.R.S.B.)
[3] Potiguar University, Laureate International Universities, School of Information Technology and Engineering, 59082-902, Natal RN, Brazil; catarina.coriolano@gmail.com (A.C.F.C.)
[4] University of Málaga, Faculty of Sciences, Department of Inorganic Chemistry, Crystallographic and Minieralogy, CP 29071, Malaga, Spain; alvarorcarmona@gmail.com (A.R.C.); castellon@uma.es (E.R.C.)
* Correspondence: mnbarbosa@gmail.com, araujo.ufrn@gmail.com; Tel.: +55-84-3211-9240

Abstract: The adsorption of carbon dioxide on amino silanes-functionalized MCM-41 and SBA-15 materiais is reported. The functionalization of mesoporous silicas was made by post-synthesis method, by impregnation of 3-aminopropyltriethoxysilane. The obtained materials were characterized by X-ray diffraction, scanning and transmission electron microscopies, nitrogen adsorption-desorption and X-ray photoelectron spectroscopy measurements. The carbon dioxide adsorption capacities for the samples were carried out under ambient pressures. The obtained results evidenced that amino-silanes with a terminal amine (–NH_2) were functionalized through covalent coupling of this group on the surface of the channels in the ordered mesoporous silica, meaning that the amine is anchored on the surface of the bigger pores of the MCM-41 and SBA-15 support. For functionalized materials, the CO_2 adsorption capacity of the AMCM-41 increased from 0.18 to 1.1 mmol g^{-1}, whereas for ASBA-15, it was from 0.6 to 1.8 mmol g^{-1}. The Lagergren kinetic algorithms were applied in order to validate the obtained results, evidencing the enhanced carbon dioxide adsorption capacity and stability of the functionalized ordered mesoporous molecular sieves.

Keywords: Adsorption; 3-Aminopropyltriethoxysilane; Carbon dioxide; Functionalization; Mesoporous silica; MCM-41; SBA-15

1. Introduction

The increase in the atmospheric carbon dioxide concentration is becoming a serious environmental problem. It is well known that the main human activity that emits CO_2 is the combustion of fossil fuels (coal, natural gas, and oil) for energy and transportation, although certain industrial processes and land-use changes also emit CO_2. In the transition towards a more sustainable energy economy, fossil fuels are likely to remain the main source of global energy supply for the future [1,2]. Thus, the continuous use of fossil fuels is dependent on the reduction of CO_2 emissions. Improving the efficiency of energy utilization and increasing the use of low-carbon energy sources are considered to be potential ways to reduce CO_2 emissions. Recently, carbon capture and storage (CCS) techniques have been proposed as an emerging technology to effectively minimize CO_2 emissions [3].

 doi:10.20944/preprints201809.0605.v1

The most common technologies for CO_2 scrubbing from power plant flue gas are on the basis of adsorption, using liquid amines. The major drawbacks of these adsorbents are the large amount of energy required for regeneration, equipment corrosion, and solvent degradation in the presence of oxygen [4]. Therefore, in the last years many efforts and funding have been focused on the development of alternative procedures for CO_2 capture, such as cryogenic technologies, adsorption or membrane based techniques [5,6]. Because of the low energy requirement, cost advantage, and ease of applicability over a relatively wide range of temperatures and pressures, adsorption separation attracts much interest.

The most important element of the chemical adsorption of CO_2 involves the design and development of a suitable adsorbent which consist of a porous support onto which an amine is attached [7]. The adsorption of carbon dioxide has been studied in various mesoporous materials including the MCM-41 and SBA-15 [8-11]. Groups of researchers have been trying to introduce amine groups into mesoporous silicas because of their elevated surface area. Polyethanolamine has been a modifying alternative for MCM-41 type materials, greatly improving the efficiency of the amine for CO_2 adsorption [12]. The CO_2 adsorption capacity of this adsorbent modifying is 24 times more than that of MCM-41. The use of amino groups anchored to a solid support greatly reduces the potential toxic and corrosive and makes easier the process of regeneration. Mesoporous silicas with different pore size were modified by aminosilanes and CO_2 adsorption capacity was improved. However, (3-trimethoxysilylpropyl) diethylentriamine (TA) modified mesoporous silicas with small pores such as MCM-41 (2.9 or 3.1 nm) and SBA-15 (6.2 or 7.1 nm) were significantly decreased at high aminosilane density. In contrast, modified SBA-15 with a large pore (10.6 nm) exhibited further improvement of CO_2 adsorption capacity and amine efficiency [13].

According literature [14], mesoporous molecular sieves MCM-41 was modified by impregnation with polyethyleneimine (PEI) and CO_2 adsorption properties of these materials were found to depend on the kind and amount of the organic compound loaded. Grafted samples showed amine efficiencies in CO_2 capture up to 0.38 mol CO_2/mol N, leading to CO_2 uptakes ranging from 38.2 to 76.9 mg CO_2/g ads (pure CO_2, 45 °C, 1 bar) [14]. The key issue for adsorption separation is to develop an adsorbent with high CO_2 adsorption capacity and high CO_2 selectivity.

The aim of this works is to incorporate aminopropyltriethoxysilane (abbreviated as APTES) in the MCM-41 and SBA-15 mesoporous materials, in order to improve their adsorption capacities for CO_2, focusing to reduce the emissions greenhouse gases in the atmosphere.

2. Materials and Methods

The ordered mesoporous molecular sieves MCM-41 and SBA-15 were synthesized by hydrothermal method according to the studies of literature [15,16]. Synthesis by the hydrothermal method was carried out in 200 mL Teflon containers introduced inside the system (autoclave stainless), under heating at 100 °C. In the synthesis of MCM-41 was used as reagents precursors, silica gel as a silicon source, sodium hydroxide as sodium source, cethyltrimethylammonium bromide (CTABr) as template structure and distilled water as solvent. The gel was prepared with the following composition in grams: 17.1125 CTMABr / 3.7348 NaOH / 11.6835 SiO_2 / 165 H_2O. The solution containing sources of silica and sodium was added to an aqueous solution of CTABr. The mixture was stirred at 60 °C for 2 hours and this reactive hydrogel was transferred to a Teflon-lined stainless steel autoclave, which were kept at 100 °C during 96 hours. The obtained material was filtered, washed, dried at 100 °C by 4 hours and calcined in N_2 and air flow at 450 °C during 2 hours.

To obtain the SBA-15 mesoporous molecular sieve, the hydrogel was prepared with the following composition in grams: 10.4 TEOS / 4.8 P123 / 10 HCl / 174 H_2O. Other literature studies are able to obtain this material using Pluronic F127 and phenolic resin oligomers (resol) as precursors, however, the quantities in grams of these reagents were much higher compared to this work [17,18]. In this way, the choice of precursors and their quantities allowed lowering the synthesis cost. The mixture was stirred at 40 °C for 24 hours, it was transferred to a Teflon-lined stainless steel autoclave, which were kept at 100 °C during 48 hours. The precipitate was filtered, washed and dried at 100 °C

 doi:10.20944/preprints201809.0605.v1

overnight. To remove the structure-directing agent, the dried precipitate was calcined in air at 550 °C for 6 hours.

The calcined MCM-41 and SBA-15 materials were functionalized by post-synthesis method, using a system reflux for impregnation of the APTES amine. Initially, the MCM-41 and SBA-15 were previously dried at 100 °C under N_2 flow during 2 hours. Afterwards, 1 g of the mesoporous material were added to the mixture containing APTES (3 mL) and ethanol (30 mL), and submitted to reflux at 75 °C for 24 hours. After, the products were filtered and washed several times with ethanol, and dried at 100 °C overnight. The obtained samples were labeled as AMCM-41 and ASBA-15, relative to MCM-41 and SBA-15 after grafting with 3-aminopropyl-triethoxysilane, respectively.

The X-ray diffraction (XRD) patterns were obtained with a Philips Xpert PRO apparatus using Cu $K\alpha_1$ radiation (λ = 0.1540 nm) with Ge (111) monochromator working at 45 kV and 35 mA. All the measurements were made with a step size of 0.0167 degree in 30 minutes. Scanning electron microscopy (SEM) micrographs were obtained by using a JEOL SM 840 microscope, working at 15 kV. Samples were placed on an aluminum drum and metalized with a gold film using a JEOL Ion Sputter JFC 1100. Transmission electron microscopy (TEM) images were obtained with a Philips CM 200 microscope working at 100 kV. The measurements of energy dispersive X-ray spectroscopy were registered using an EDAX CM200ST probe based in a detector SiLi. The samples were dispersed in 2-propanol and dropped over a Cu grid.

Nitrogen adsorption-desorption measurements were performed at liquid N_2 temperature (77 K) with an ASAP 2020 apparatus from Micromeritics. Before each measurement, samples were degassed by 12 hours at 423 K and 10^{-2} Pa. The specific BET surface area (S_{BET}) was calculated using the BET equation, and the specific pore volume (Vp) was calculated at P/P_0 = 0.98. The pore size distribution was calculated following BJH method, taking the data of the desorption branch and assuming a cylindrical pore model.

The X-ray photoelectron spectroscopy (XPS) studies were realized by a Physical Electronic PHI 5700 spectrometer using non monochromatic Mg K radiation (300W, 15 kV, 1253.6 eV) for the analysis of the core level signals of C 1s, N 1s, O 1s and Si 2p with a hemispherical multichannel detector. The binding energy values were referenced to C 1s signal (284.8 eV). Shirley type background and Gauss-Lorentz curves were used to determinate the binding energy.

The CO_2 adsorption tests consisted of two steps: the activation and adsorption. A mass sample of ca. 100 mg were transferred to a glass sample holder, contained within the reactor, and subjected to activation step into a stream of N_2, approximately 150 mL min^{-1} for 2 hours at a temperature of 200 °C. After activation, the system was cooled to room temperature and then performed the adsorption step. Before starting the adsorption, the adsorbent was weighted again. The adsorption was carried out under atmospheric pressure and CO_2 flowing at 150 mL min^{-1}, at room temperature and variation in reaction time from 0 to 210 minutes. The adsorption capacity was calculated according to the weight variation observed to reach equilibrium as being equal to the ratio of the amount of CO_2 adsorbed by the adsorbent mass activated.

The adsorption kinetics were described by kinetic models of pseudo first and second-order. The linear form of the models are given by Lagergren equations (1) and (2) [19,20].

$$\log (q_e - q_t) = \log q_e - (K_1 / 2.303)\, t \quad (1)$$

$$t / q_t = 1 / (K_2\, q_e^2) + (1 / q_e)\, t \quad (2)$$

The values of K_1 can be obtained from the slope of the plot of $\log (q_e - q_t)$ versus t. The plot of t / q_t versus t gives a linear relationship, allowing for computation of q_e and K_2. The validity can again be tested by comparing values of q_e obtained from the plots and from experiments [21].

3. Results and Discussion

 doi:10.20944/preprints201809.0605.v1

148 *3.1. Materials Characterization*

149 3.1.1. X-Ray diffraction

150 The APTES-functionalized mesoporous molecular sieves MCM-41 and SBA-15, before and after
151 surface modification, were characterized by XRD and the results are compared in Figs. 1 and 2,
152 respectively. The XRD patterns of MCM-41 (Fig. 1(a)) and AMCM-41 (Fig. 1(b)) are consistent with
153 the literature, showing one large peak corresponding the plane (100), along with three small peaks of
154 the planes (110), (200) and (210), which are typical features of MCM-41 materials [22,23]. The same
155 behavior was observed with SBA-15 and ASBA-15 materials, that presented the diffraction peaks
156 characteristic to mesoporous silicas in the plans (100), (110), and (200), as shown in Fig. 2(a) and Fig.
157 2(b) for SBA-15 and ASBA-15, respectively. The structures of mesoporous materials after
158 functionalization were preserved.

159

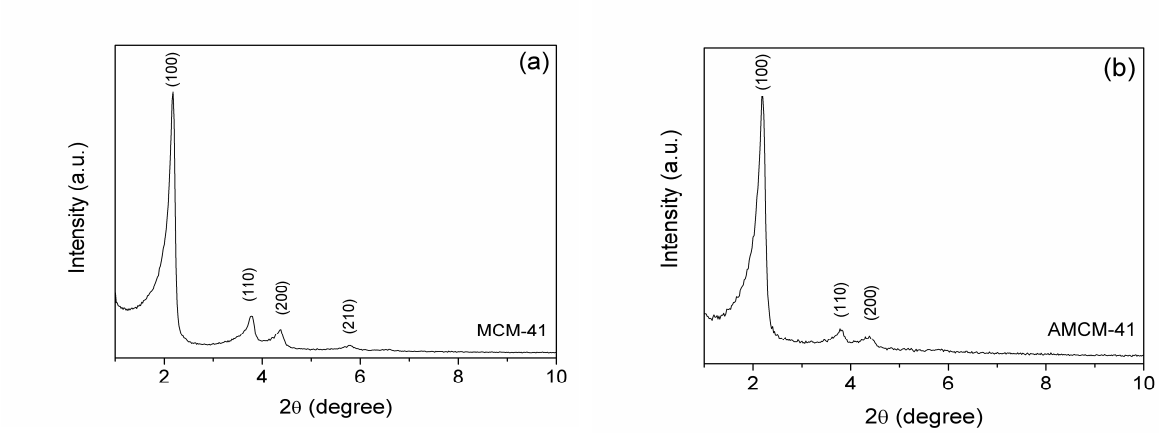

160 **Figure 1.** 1 Low-angle X-ray diffraction spectra of the synthesized materials: (a) MCM-41 and (b)
161 AMCM-41 (MCM-41 after grafting with 3-aminopropyl-triethoxysilane).

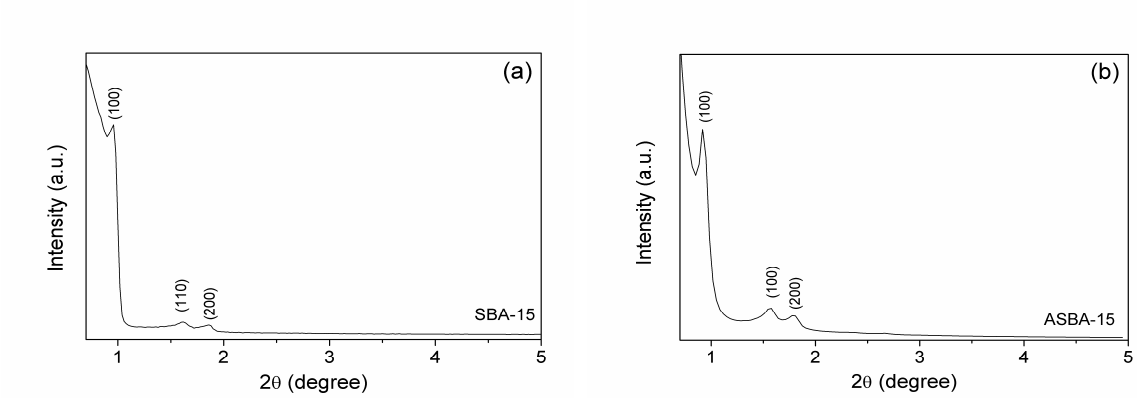

162 **Figure 2.** Low-angle X-ray diffraction spectra of the synthesized samples: (a) SBA-15 and (b) ASBA-
163 15 (SBA-15 after grafting with 3-aminopropyl-triethoxysilane).

164 3.1.2. SEM and TEM analysis

165 Analyses of SEM of the synthesized and functionalized samples are presented in Fig. 3. This
166 technique was used in order to observe the morphology of materials obtained. According to the
167 micrographs, the synthesized materials were formed by agglomeration of particles generally
168 rounded. Moreover, for samples AMCM-41 and ASBA-15 (Fig. 3(d) and 3(b)), the morphology of

 doi:10.20944/preprints201809.0605.v1

particles were similar when compared with the morphology of the synthesized material, MCM-41 and SBA-15 (Fig. 3(c) and 3(a)).

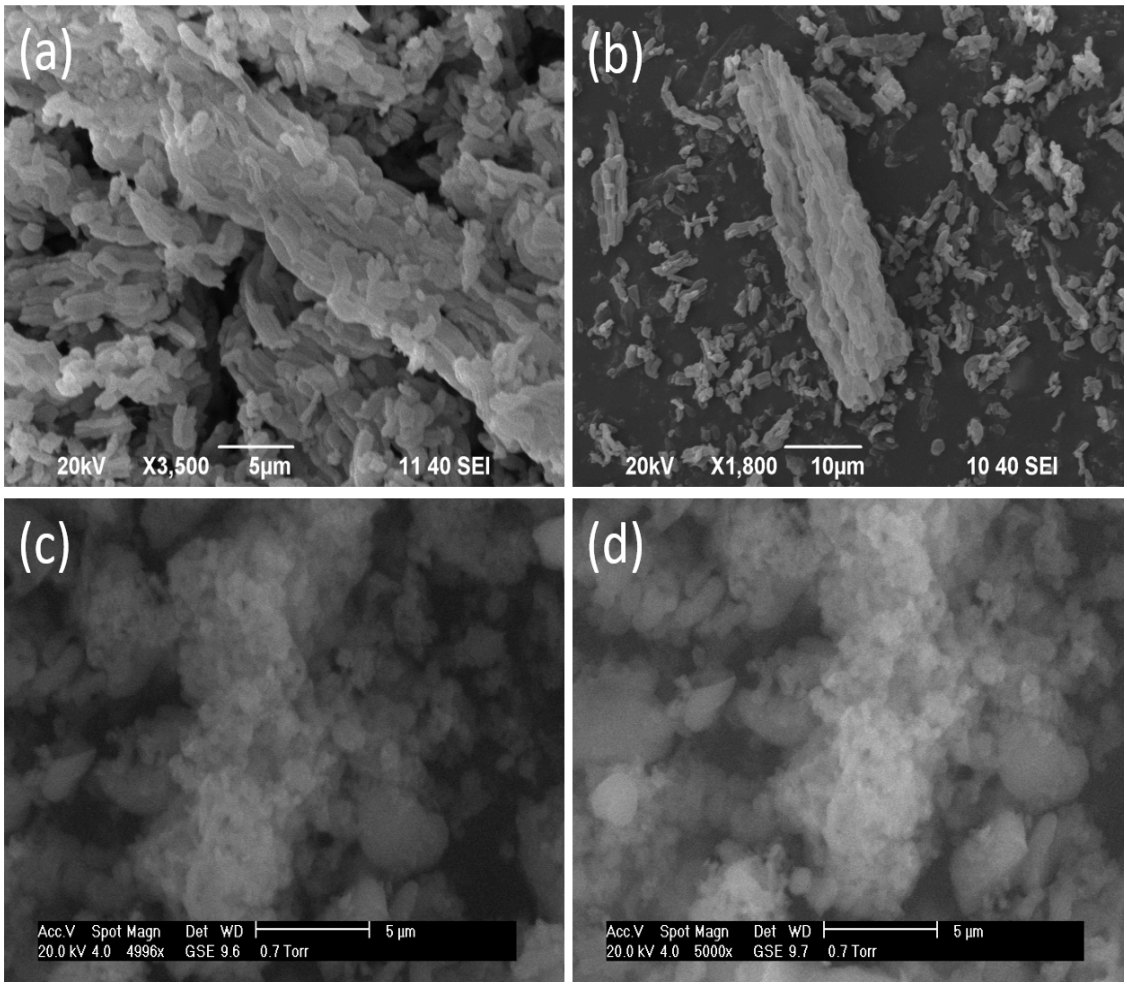

Figure 3. SEM images for samples (a) SBA-15 (×3.500), (b) ASBA-15 (×1.800), (c) MCM-41 (×4.996) and (d) AMCM-41 (×5.000).

The mesopores hexagonal structure of these materials cannot be observed through this analysis technique, because it does not provide an image resolution that reveals visually mesoporous hexagonal channels, as well as their lateral silica tubes. The technique that shows the exact structure for this type of material is TEM.

The TEM of the synthesized MCM-41 and SBA-15 materials (Fig. 4(a) and 4(c)) showed the characteristic structures of mesoporous materials, since the formation of hexagonal ordered mesoporous and shows the high quality of material obtained. Besides the hexagonal mesoporous, we observed silica tubes formed in parallel. This result is directly correlated with the XRD technique, in which, the presence of the diffraction peak related to the plane (100) corresponds to the tubular channels formed by silica material. The same mesoporous structures were observed for samples functionalized AMCM-41 and ASBA-15 (Fig. 4(b) and 4(d)), without compromising their structure even after functionalization with the amine. The functionalized materials maintained their hexagonal formation, as well as the ordering of their silica tubes.

 doi:10.20944/preprints201809.0605.v1

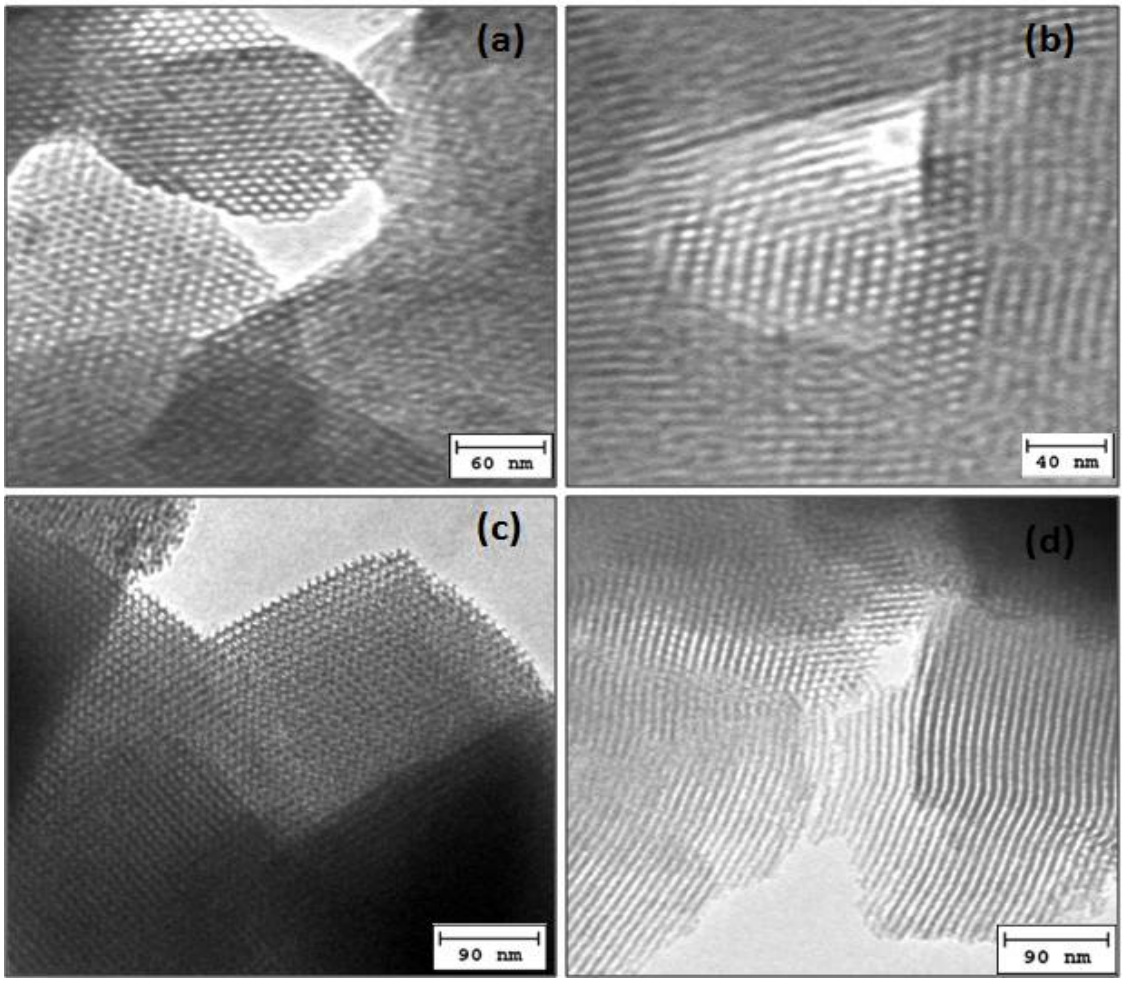

Figure 4. TEM image showing highly ordered, long-range hexagonal array of mesopores in the obtained materials before and after modification with amino silanes: (a) MCM-41, (b) AMCM-41, (c) SBA-15 and (d) ASBA-15.

3.1.3. N_2 adsorption/desorption isotherms

Nitrogen adsorption/desorption isotherms of the materials studied are shown in Fig. 5. All the samples have the type-IV isotherm, following the recommendations of IUPAC [24] with a H1 hysteresis loop that is representative of mesoporous materials [25]. The isotherms of the samples have a sharp capillary condensation step. The parameters of the porous structure and XRD data are summarized in Table 1.

The MCM-41 and SBA-15 exhibit high values of surface area (S_{BET}), equivalent to 713 to 1070 m^2 g^{-1}, respectively. However, the functionalized samples, AMCM-41 and ASBA-15, had lower values regarding its textural properties when compared with pure materials, i.e. surface area of 465 and 666 m^2 g^{-1}, respectively.

Preprints (www.preprints.org) | NOT PEER-REVIEWED | Posted: 30 September 2018 doi:10.20944/preprints201809.0605.v1

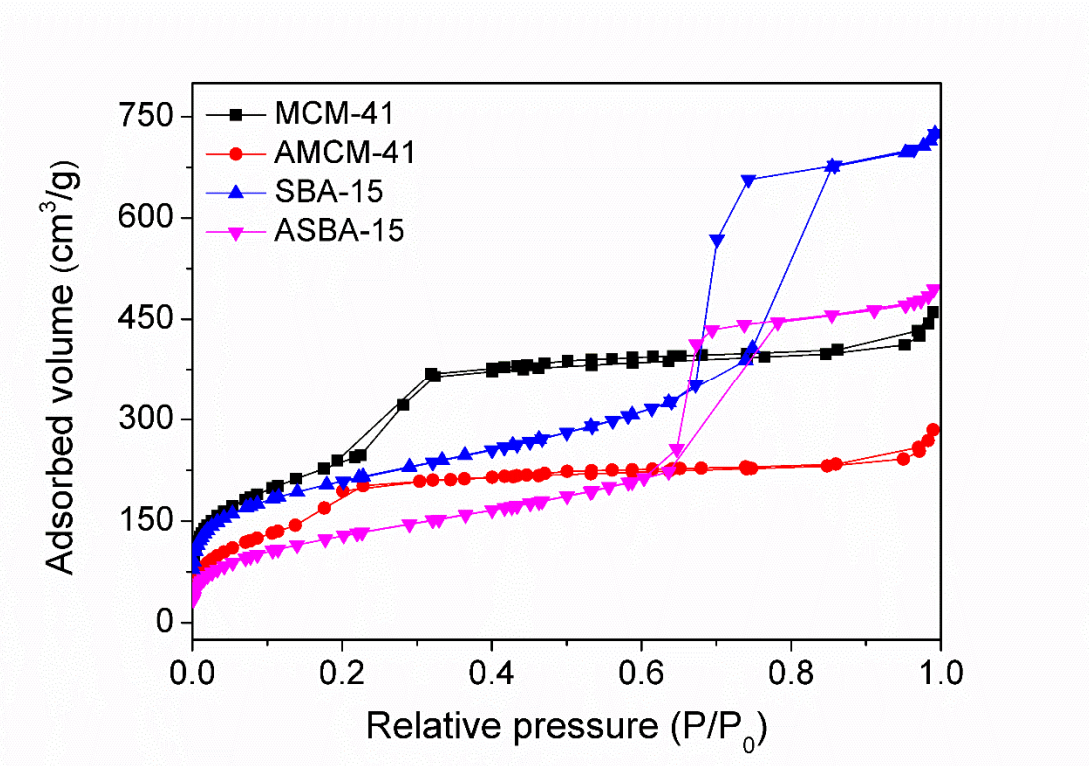

Figure 5. Nitrogen adsorption and desorption isotherms at 77 K for the MCM-41, AMCM-41, SBA-15 and ASBA-15 materials.

Table 1. Textural properties of the obtained materials before and after amino silanes surface modification.

Materials	a_0 (nm)	Dp (nm)	Wt (nm)	Vp ($cm^3\ g^{-1}$)	S_{BET} ($m^2\ g^{-1}$)
MCM-41	4.85	2.8	2.0	0.81	1070
SBA-15	12.43	6.4	6.0	1.08	713
AMCM-41	4.63	1.9	2.7	0.43	666
ASBA-15	11.10	4.3	6.8	0.76	465

a_0: Lattice spacing, Dp: pore diameter, Wt: wall thickness (Wt = a_0 - Dp), Vp: pore volume, S_{BET}: surface area

3.1.5. XPS analysis

The results concerning the characterization by XPS of the synthesized mesoporous materials are given in Table 2. According to the data, it was possible to obtain the atomic composition of the elements present in the materials. A much greater concentration of the nitrogen element was

Preprints (www.preprints.org) | NOT PEER-REVIEWED | Posted: 30 September 2018 doi:10.20944/preprints201809.0605.v1

observed for the functionalized samples as compared to the non-functionalized samples, since the latter are not present in their elemental composition the nitrogen atom. Thus, this composition of the nitrogen element evidenced the presence of amine groups in these materials.

Table 2. Atomic concentrations of the elements in the synthesized materials.

Materials	C 1s	N 1s	O 1s	Si 2p	C – C_a / N	O / Si
MCM-41	4.95	0.18	64.1	30.8	-	2.08
AMCM-41	17.3	2.25	53.4	27.0	5.49	1.97
SBA-15	5.62	0.16	63.2	31.1	-	2.03
ASBA-15	15.6	2.52	53.5	28.3	3.96	1.88

The Fig. 6(a) and 6(b), shows the XPS electronic spectra, individually, for the APTES whit functionalized samples, AMCM-41 and ASBA-15, respectively. Analyzing these spectra, for both samples, the N 1s peaks related to the nitrogen element were evidenced. The most intense peak is superimposed on another intense peak with noises that is called the original peak. Therefore, only the two peaks (more intense and less intense), corresponding to the peaks of N 1s and their two energies of bonds detected by XPS (399.4 eV and 401.5 eV) were taken into account. These two energies were attributed the N-H and N-C bonds, respectively. Therefore, this technique proves the presence of the amine in these materials through the XPS spectra.

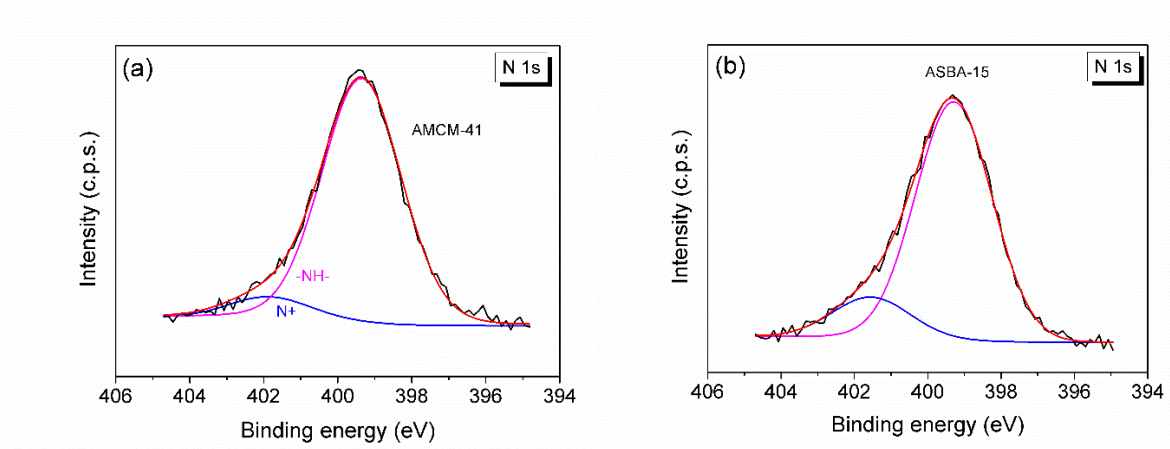

Figure 6. XPS spectrum N 1s of (a) AMCM-41 and (b) ASBA-15 samples.

3.2. CO_2 Adsorption

To evaluate the potential of the obtained materials as adsorbents for CO_2 capture, Fig. 7 shows the curves of adsorption of carbon dioxide materials. It was observed that the MCM-41 and SBA-15 showed low adsorption capacity for CO_2 compared to materials functionalized with APTES. The graph corresponding to the amount of CO_2 adsorbed versus time showed the isotherms for ASBA-15 and AMCM-41 samples, since their adsorption capacities have been improved from 0.6 and 0.1 mmol g^{-1}, respectively, to reaching 1.8 and 1.0 mmol g^{-1}. These adsorption improvements show the influence of amino groups in the structure of mesoporous materials, favoring the adsorption process.

Preprints (www.preprints.org) | NOT PEER-REVIEWED | Posted: 30 September 2018 doi:10.20944/preprints201809.0605.v1

In addition, these adsorption capacities were higher when compared with other similar works in the literature [26,27]. Another relevant factor is that the adsorption process was carried out at atmospheric pressure (1 atm) and at room temperature (30 °C), with a variation in adsorption time from 0 to 210 minutes. These conditions can be adjusted to improve the adsorption capacities, since an increase in the adsorption temperature or pressure may favor the capacity of the material [27].

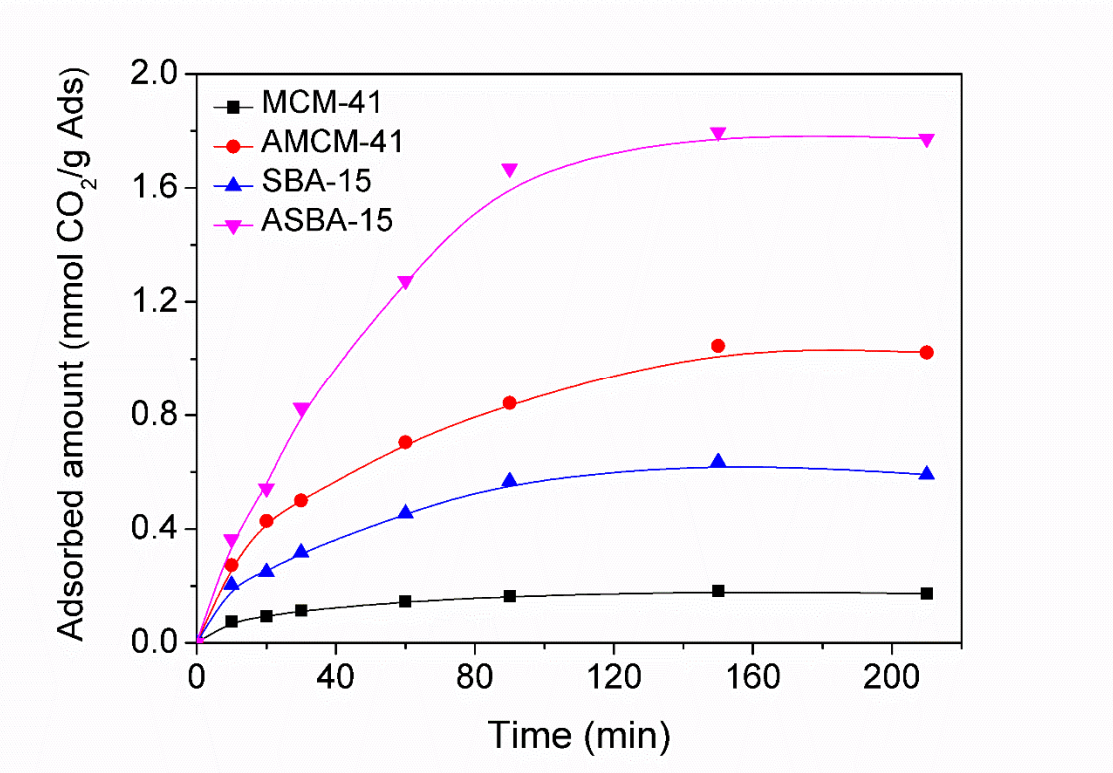

Figure 7. CO_2 adsorption capacities of the obtained materials, obtained at room temperature.

3.3. Kinetic Study

From the results of adsorption of CO_2 for various times, curves were constructed representing the kinetics of sorption of CO_2 by mesoporous materials. The graphs referring to kinetic models pseudo first-order, log (q_e–q_t) versus time, and the pseudo second-order, t/q_t versus time, are shown in Fig. 8(a) and 8(b), respectively. Table 3 shows the kinetic parameters obtained by linear regressions of these graphs. Quantitative evaluation of models requires that the correlation coefficients are compared (R^2). It was observed that the R^2 values calculated for the kinetic model of pseudo second-order greater were than 0.99. Another relevant parameter was the calculated q_e values. Since the calculated values of q_e are greater than the experimental values of q_e, this one shows a consistency of results, otherwise, if the calculated values of q_e are lower than the experimental values, they are not relevant. The results of adsorption did not fit the kinetic model of first-order by this fact. However, the CO_2 adsorption experiments were best fitted to the engine pseudo second-order, since this adjustment was confirmed by comparing of the experimental q_e values with the calculated, which showed in good agreement.

Preprints (www.preprints.org) | NOT PEER-REVIEWED | Posted: 30 September 2018 doi:10.20944/preprints201809.0605.v1

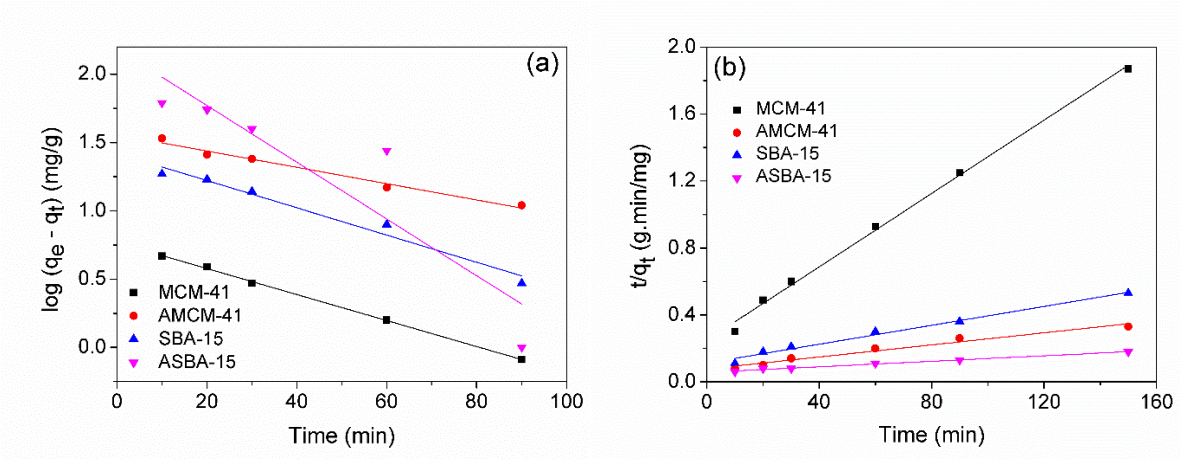

(**a**) (**b**)

Figure 8. Kinetic analysis of the CO2 adsorption of materials studied at room temperature by (a) Lagergren pseudo first-order (LFO) equation and (b) pseudo second-order (PSO) equation.

Table 3. Kinetic parameters of the CO_2 adsorption of materials studied by Lagergren pseudo first-order equation and pseudo second-order equation

Kinetic		MCM-41	SBA-15	AMCM-41	ASBA-15
First-order*	K_1	0.022	0.022	0.013	0.047
	R^2	0.99	0.96	0.97	0.97
	a	0.76818	1.42023	1.55682	2.18579
	b	–0.00953	–0.00996	–0.00597	–0.02076
	q_e experimental	8	28	46	79
	q_e calculated	6	26	36	151
Second-order**	K_2	6.2×10^{-3}	1.1×10^{-3}	6.2×10^{-4}	2.8×10^{-4}
	R^2	0.99	0.99	0.99	0.99
	a	2.49319	1.12381	0.76129	0.56262
	b	0.10984	0.02821	0.01773	0.00843
	q_e experimental	8	28	46	79
	q_e calculated	9	35	56	118

*$\log(q_e–q_t) = \log(q_e)–(K_1/2{,}303)t$; **$t/q_t = 1/(K_2q_e^2) + (1/q_e)t$; coefficients : a, b.

4. Conclusions

Amino silanes-functionalized mesoporous molecular sieves MCM-41 and SBA-15 type were prepared by post-synthesis functionalization via a facile reflux method. Through physico-chemical characterizations of the synthesized materials before and after modification with amine, it was possible to evaluate the efficiency of the functionalization method, showing the presence of amino groups in the structure of mesoporous molecular sieves, according to the XPS analysis. The CO_2 adsorption tests showed an increase in the amount of gas adsorbed on both samples containing

 doi:10.20944/preprints201809.0605.v1

amine, reaching 1.1 mmol g^{-1} for sample AMCM-41 and 1.8 mmol g^{-1} for sample ASBA-15. It was possible to compare the quantities adsorbed experimentally and theoretically through kinetic studies and thereby validate the adsorption experiments. The kinetic parameters obtained were best fitted to the kinetic model of second order, since the calculated values of q_e were consistent compared with the experimental values, as well as the correction factor equal to 0.99. It is important to note that the CO_2 adsorption process was carried out at room temperature under atmospheric pressure. The results are relevant for such materials and can be improved by varying the condition of the adsorption process at higher pressures or temperatures.

Author Contributions: Conceptualization on mesoporous materials for gas adsorption, M.N.B*. and M.N.B.; experimental methodology for synthesis and modification of adsorbents, M.J.F.C and J.R.S.B.; characterization of the materials by SEM, TEM and XPS, A.R.C. and E.R.C.; resources, some reagents and tools, V.J.F.; writing—original draft preparation, M.N.B*.; writing, review and editing, A.C.F.C. and A.S.A.

Acknowledgments: The authors thank the Brazilian Agency of Petroleum, Natural Gas and Biofuel (ANP), and National Council for Scientific and Technological Development (CNPq Brazil, Grant number 311136/2014-1), CAPES and MICINN (MAT2009-10481) from Spain and European FEDER funds for financial support. This work is result of a Brazil-Spain research cooperation.

Conflicts of Interest: The authors declare no conflict of interest.

References and Notes

1. Beckman, E.J. Supercritical and near-critical CO2 in green chemical synthesis and processing. *J. Supercrit Fluid* **2004**, *28*, 121–191.
2. Corfee-kmjjMorlot, J.; Höhne, N. Climate change: long-term targets and short-term commitments. *Global Environmental Change* **2003,** *13*, 277–293.
3. Zhou J.; Zhao, H.; Li, J.; Zhu, Y.; Hu, J.; Liu, H.; Hu, H. CO_2 capture on micro/mesoporous composites of (zeolite A)/(MCM-41) with Ca^{2+} located: Computer simulation and experimental studies. *Solid State Sciences* **2013**, *24*, 107–114.
4. Du, R.; Feng, X.; Chakma, A. Poly(N,N-dimethylaminoethyl methacrylate)/polysulfone composite membranes for gas separations. *J. Membrane Sci.* **2006**, *279*, 76–85.
5. Tajnik, T.; Bogataj, L.K.; Jurač, E.; Lasnik, C.R.; Likar, J.; Debelak, B. Investigation of adsorption properties of geological materials for CO_2 storage. *Int. J. Energy Res*. **2013,** *37*, 952–958.
6. Yu, C.; Huang, C.; Tan, C. A review of CO_2 capture by absorption and adsorption. *Aerosol and Air Quality Research*. **2012**, *12*, 745–769.
7. Ünveren, E.E.; Monkul, B.O.; Sarıoglan, S.; Karademir, N.; Alper, E. Solid amine sorbents for CO2 capture by chemical adsorption: A review. *Petroleum* **2017**, *3*, 37-50.
8. Carvalho, L.S.; Silva, E.; Andrade, J.C.; Silva, J.A.; Urbina, M.; Nascimento, P.F.; Carvalho, F.; Ruiz J.A. Low-cost mesoporous adsorbents amines-impregnated for CO_2 capture. *Adsorption* **2015**, *21*, 597–609.
9. Jing, Y.; Wein, L.; Wang, Y.; Yu, Y. Synthesis, characterization and CO2 capture os mesoporous SBA-15 adsorbents functionalized with melanine-based and acrylate-based amine dendrimers. *Micropor Mesopor Mater*. **2014**, *183*, 124–133.
10. Montagnaro, F.; Silvestre-Albero, A.; Silvestre-Albero, J.; Rodríguez-Reinoso, F.; Erto, A.; Lancia, A.; Balsamo, M. Post-combustion CO_2 adsorption on activated carbons with diferente textural properties. *Micropor Mesopor Mater*. **2015**, *209*, 157–164.
11. Vilarrasa-García, E.; Cecilia, J.A.; Bastos-Neto, M.; Cavalcante Jr, C.L.; Azevedo, D.C.S.; Rodríguez-Castellón, E. CO_2/CH_4 adsorption separation process using pore expanded mesoporous sílicas functionalizated by APTES grafting. *Adsorption* **2015**, *21*, 565–575.
12. Balaraman, E.; Gunanathan, C.; Zhang. J.; Shimon, L.J.W.; Milstein, D. Efficient hydrogenation of organic carbonates, carbamates and formates indicates alternative routes to methanol based on CO_2 and CO. *Nature Chem*. 2011, *3*, 609–614.
13. Hori, K.; Higuchi, T.; Aoki, Y.; Miyamoto, M.; Oumi, Y.; Yogo, K.; Uemiya, S. Effect of pore size, aminosilane density and aminosilane molecular length on CO_2 adsorption performance in aminosilane modified mesoporous silica. Microp. Mesop. Mater. **2017**, *246*, 158-165.

14. Sanz, R.; Calleja, G.; Arencibia, A.; Sanz-Pérez, E.S. CO_2 Capture with pore-expanded MCM-41 silica modified with amino groups by double functionalization. *Micropor Mesopor Mater*. **2015,** *209*, 165–171.
15. Araujo, A.S.; Jaroniec, M. Thermogravimetric monitoring of the MCM-41 synthesis. *Thermochimica Acta* **2000**, *363*, 175–180.
16. Zhao, D.; Huo, Q.; Feng, J.; Chmelka, B.F.; Stucky, G.D. Nonionic Triblock and Star Diblock Copolymer and oligomeric surfactant syntheses of highly ordered, hydrothermally stable, mesoporous silica structures. *J. Am. Chem. Soc.* **1998**, *120*, 6024–6036.
17. Qiang, Z.; Guo, Y.; Liu, H.; Cheng, S.Z.D.; Cakmak, M.; Cavicchi, K.A.; Bogt, B.D. Large-scale roll-to roll fabrication of ordered mesoporous materials using resol-sssisted cooperative assembly. *Appl. Mater. Interfaces* **2015,** *7*, 4306−4310.
18. Qiang, Z.; Gurkan, B.; Ma, J.; Liu, X.; Guo, Y.; Cakmak, M.; Cavicchi, K.A.; Vogt, B.D. Roll-to-roll fabrication of high surface area mesoporous carbon with process-tunable pore texture for optimization of adsorption capacity of bulky organic dyes. *Micropor Mesopor Mater*. **2016,** *227*, 57−64.
19. Ayyappan, R.; Sophia, A.C.; Swaminathan, K.; Sandhya, S. Removal of Pb(II) from aqueous solution using carbon derived from agricultural wastes. *Process Biochemistry* **2005,** *40*, 1293–1299.
20. Yuh-Shan, H. Citation review of Lagergren kinetic rate equation on adsorption reactions. *Scientometrics* **2004**, *59*, 171–177.
21. Ho, Y.S.; McKay, G. Batch lead (II) removal from aqueous solution by peat: Equilibrium and kinetics. *Proc Safe Environ Protec*. **1999**, *77*, 165–173.
22. Beck, J.S.; Vartuli, J.C.; Roth, W.J.; Leonowicz, M.E.; Kresge, C.T.; Schmitt, K.D.; Chu, C.T.W.; Olson, D.H.; Sheppard, E,W.; McCullen, S.B.; Higgins, J.B.; Schlenker, J.L. A new family of mesoporous molecular sieves prepared with liquid crystal templates. *J. Am. Chem. Soc.* **1992**, *114*, 10834–10843.
23. Kresge, C.T.; Leonowicz, M.E.; Roth, W.J.; Vartuli, J.C.; Beck, J.S. Ordered mesoporous molecular sieves synthesized by a liquid-crystal template mechanism. *Nature* **1992,** *359*, 710–712.
24. Gregg, S.J.; Sing, K.S.W. *Adsorption, Surface Area, and Porosity*. 2nd ed. New York, Academic Press. **1982.**
25. Chareonpanich, M.; Nantangern, A.; Limtrakul, J. Short-period synthesis of ordered mesoporous silica SBA-15 using ultrasonic technique. *Mater Lett*. **2007,** *61*, 5153–5156.
26. Ma, X.; Wang, X.; Song, C. Molecular basket sorbents for separation of CO_2 and H_2S from various gas streams. *J. Amer. Chem. Soc.* **2009**, *131*, 5777–5783.
27. Xu, X.; Song, C.; Andrésen, J.M.; Miller, B.G.; Scarone, A.W. Preparation and characterization of novel CO_2 molecular basket adsorbents based on polymer-modified mesoporous molecular sieve MCM-41. *Micropor Mesopor Mater*. **2003**, *62*, 29–45.